

**Fatigue Pre-Cracking Curved Wide Plates in Bending\***

**Mark D. Richards**

National Institute of Standards and Technology  
**Boulder, CO, USA**

**Timothy S. Weeks and J. David McColskey**  
National Institute of Standards and Technology  
**Boulder, CO, USA**

**Bo Wang and Yong-Yi Wang**  
Center for Reliable Energy Systems  
**Dublin, OH, USA**

**ABSTRACT**

Curved wide plate (CWP) testing in tension, on API 5L X100 pipes of 36-inch (916-mm) diameter and 0.75-inch (19-mm) wall thickness, has been initiated in support of strain-based design using high strength steel for oil and gas pipeline applications. The CWP tests are being used to optimize and validate welding procedures and to determine the defect tolerance within the girth welds. A traditional pre-requisite for fracture mechanics testing is a final extension of a crack via fatigue pre-cracking to produce a representative flaw. A method of fatigue pre-cracking CWP specimens for final notch preparation in bending was developed to meet ASTM guidelines for fracture mechanics testing. Fatigue pre-cracking for the present specimen geometry was possible in bending due to lower requisite force capacity equipment which allowed for greater cyclic loading frequencies. In order to achieve sufficient stress levels for fatigue crack growth in the curved plate, a stress field analysis was performed to optimize the loading support configuration in four-point bending. In addition to the stress field analysis, a 3-D finite element model of the CWP specimen was generated to analyze the notched CWP specimen in four-point bending. Finite element analysis (FEA) results and experimental data were used to confirm the hypothesis that, under the proposed loading arrangement, the closed-form solutions for stress-intensity (K) of flat plates in bending can be used to approximate the K for CWP specimens in bending. Validation of a solution for stress-intensity factor subsequently allowed the determination of force amplitude levels for fatigue crack growth. Force and crack mouth opening displacement (CMOD) data were analyzed to correlate compliance with crack length measurements. From experimental results, a method was developed that enable the repeatable and well characterized extension of surface flaws by fatigue pre-cracking in curved wide plate specimens in bending.

**INTRODUCTION**

A research program was initiated on API 5L-X100 pipeline steel to support the shift towards a strain-based design philosophy for oil and gas transmission pipelines. The goal of this program was to evaluate the toughness and defect tolerance of girth welds and optimize the welding procedures for advanced, high strength steel grades. An additional goal was the evaluation and standardization of curved wide plate (CWP) tension tests as a medium scale fracture mechanics test which is simulative of the full scale condition<sup>[1-4]</sup>. The CWP test specimen was a full thickness pipe section or curved plate material where the gauge width was much wider than the surface flaw. Furthermore, a 4:1 ratio between the gauge length and gauge width was used to minimize the influence of gripping and specimen loading on the uniformity of strain at the flaw location. Figure 1 shows a schematic of the test section.

The initial surface notches were introduced to the weld and heat affected zone of a girth weld on the inner diameter of the specimen by electrical discharge machining (EDM). A schematic of one of the notch sizes used is shown in Figure 2. The final step in the specimen preparation was to extend the surface flaw by fatigue pre-cracking the plate to achieve a final flaw length following the fracture toughness testing guidelines set forth in ASTM E740 and ASTM E1820.

**STRESS-INTENSITY FACTOR ANALYSIS**

In order to pre-fatigue crack the plates in bending, a suitable stress and the corresponding loading arrangement to achieve said stress had to be determined. A series of experiments were conducted on a section of the X100 base-metal without a notch which had been instrumented with ten strain gages. Five gages were equally spaced along both the inner and outer diameter as shown in Figure 3. These experiments evaluated the maximum outer fiber stress at the notch location without exceeding 80 %

---

\*Contribution of an agency of the U.S. government, not subject to copyright

of the specified minimum yield strength (SMYS) of the steel at any other location in the test section.

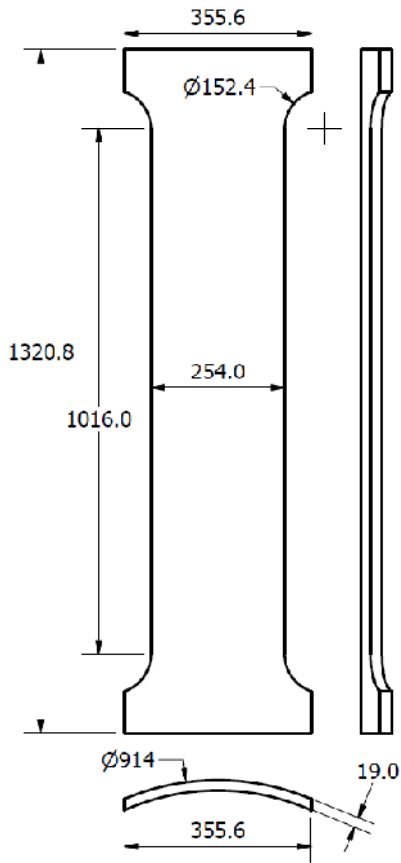


Figure 1 – Schematic of CWP test specimen pipe section without end tabs (units in mm).

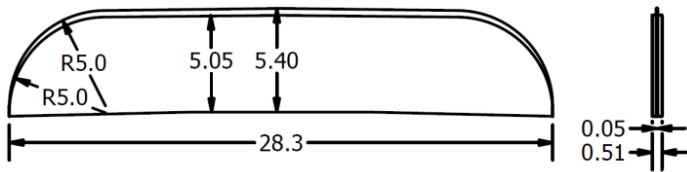


Figure 2 – Schematic of 5.4 mm deep by 28.3 mm wide CWP EDM notch (units in mm).

The following formula for determining the stress in a member under bending loads was used:

$$\sigma = \frac{My}{I_x}, \quad (1)$$

where  $M$  is the moment about the neutral  $x$  axis,  $y$  is the perpendicular distance from the location of interest to the neutral plane, and  $I_x$  is the second moment of area about the

neutral  $x$  axis.  $I_x$  was determined to be  $292 \times 10^3 \text{ mm}^4$ . The position of the neutral plane about the  $x$  axis for pure bending in the specimen coincides with the centroid of the cross section, as shown in Figure 3. In the case of four-point bending, the moment  $M$  is determined by

$$M = \frac{P}{4}(l_1 - l_2), \quad (2)$$

where  $P$  is the applied force, and  $l_1$  and  $l_2$  represent the outer and inner loading spans, respectively. In pure bending, the stress at the outer edge of the cross section on the inner diameter will be much higher than at the notch location, due to the relative proximity of the notch to the neutral plane.

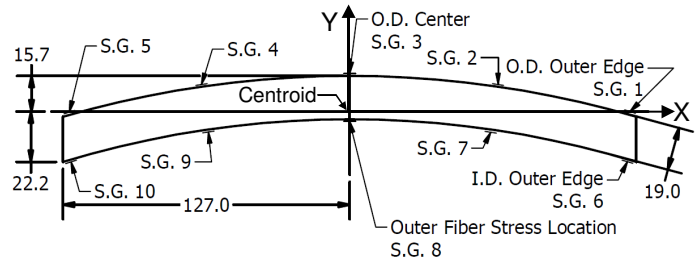


Figure 3 – Strain gage (S.G.) layout for pre-cracking stress analysis, showing the location of the centroid position for the CWP specimen cross-section (units in mm).

Two types of loading supports and multiple support spacing conditions were evaluated for four-point bending. The loading support type and inner and outer spacing settings are summarized in Table 1. The goal was to increase the outer fiber stress at the notch location without exceeding 80 % of the SMYS elsewhere in the specimen.

Table 1 – Maximum stress at notch location from strain gage data.

Test No.	Outer Span (mm)	Inner Span (mm)	Loading Support Configuration	Maximum Stress at Notch Location (MPa)	Distance of notch to neutral plane (mm)
1	279	178	Contoured Supports	112.4	4.7
2	279	114	Contoured Supports	138.6	5.7
3	279	50.8	50.8 mm $\emptyset$ – Straight Rollers	221.3	7.0
4	279	32	32 mm $\emptyset$ – Straight Rollers	333.7	7.8
5	178	32	32 mm $\emptyset$ – Straight Rollers	479.2	8.9

Contoured loading supports for both the inner diameter (I.D.), which had a convex shape, and the outer diameter (O.D.), which had a hyperbolic shape, are shown in Figure 4. Additional tests were conducted in which the outer diameter contoured supports were replaced with straight rollers of various diameters. The straight rollers were placed adjacent to each other, as shown in Figure 5. Table 1 lists the maximum

stress achieved at the notch location for each loading condition. The maximum outer fiber stress at the notch location was achieved at a force that induced a stress of 80 % of the SMYS near the outer edge of the specimen. Also listed in Table 1 are the approximate distances from the neutral plane to the inner diameter surface. Values were estimated from the peak strain data during loading from the center strain gages on the inner and outer diameter surfaces at the center of the plate and assumed that the stress was linearly variable through the thickness of the plate. Figure 6 represents the stress along the longitudinal direction of the pipe versus the distance from the inner diameter surface of the pipe for the loading configurations for test numbers 1 and 5, as listed in Table 1. The data in Table 1 show that as both support spans are minimized and the loading configuration changed from contoured supports to straight rollers on the O.D., the maximum achievable stress at the notch location significantly increased, and the neutral plane position shifted towards the center of the plate.

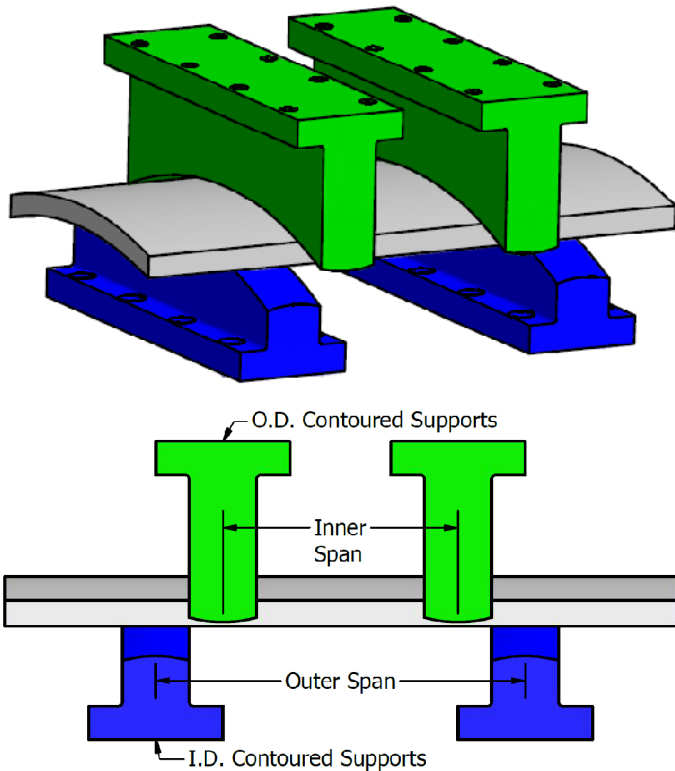


Figure 4 – Schematic of contoured support loading configuration used for tests 1 and 2 in Table 1.

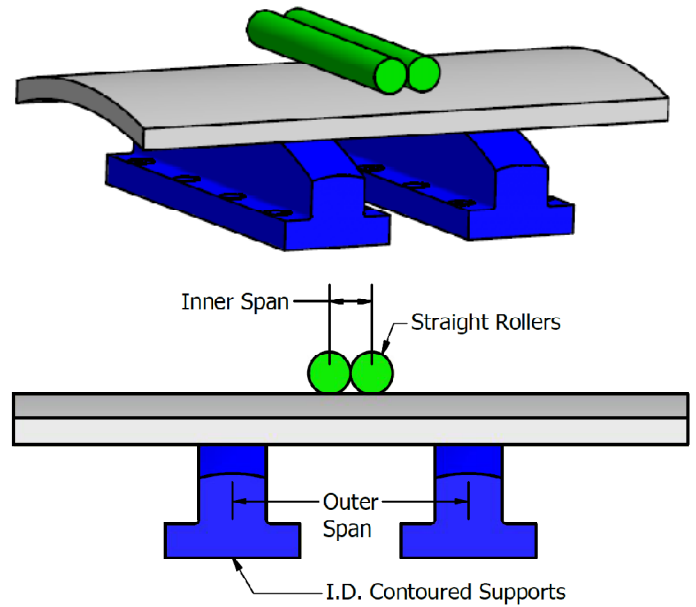


Figure 5 – Schematic of contoured support and straight rollers loading configuration as used in tests 3, 4 and 5 in Table 1.

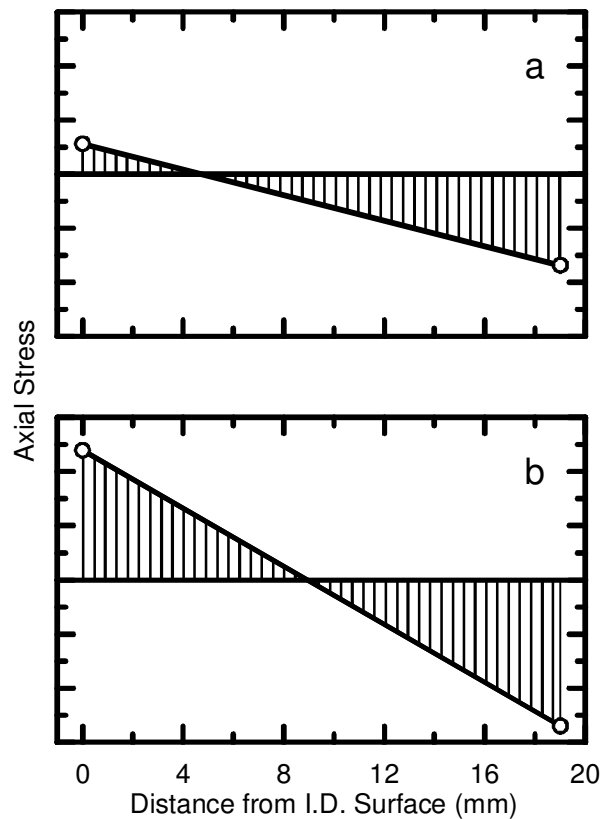


Figure 6 – Representative stress distribution through the thickness of the pipe for loading configuration 1 (a) and 5 (b). The distribution shows that the neutral plane position is closer to the plate mid-thickness in test 5 (b) than in test 1 (a).

In order to achieve optimal fatigue loading conditions and adequate fatigue crack growth rates, it was critical to identify the optimum support conditions that provided the maximum achievable outer fiber stress at the notch location. Closed form solutions for the stress-intensity factor,  $K$ , for a surface crack in a flat plate under pure bending were determined based upon ASTM E740-03, annex A2<sup>[5]</sup>. For bending with a nominal outer fiber stress  $\sigma_b$ , at the deepest point on the crack periphery,

$$K = \sigma_b \sqrt{\pi a} \left( \frac{M}{\Phi} \right) H, \quad (3)$$

where

$$M = \left\{ 1.13 - 0.09 \left( \frac{a}{c} \right) \right\} + \left\{ -0.54 + \left( \frac{0.89}{0.2 + \left( \frac{a}{c} \right)} \right) \right\} \left( \frac{a}{B} \right)^2 + \left\{ 0.5 - \frac{1}{0.65 + \left( \frac{a}{c} \right)} + 14 \left( 1 - \left( \frac{a}{c} \right)^{24} \right) \right\} \left( \frac{a}{B} \right)^4 \quad (4)$$

$$H = 1 - \left\{ 1.22 + 0.12 \left( \frac{a}{c} \right) \right\} \left( \frac{a}{B} \right) + \left\{ 0.55 - 1.05 \left( \frac{a}{c} \right)^{0.75} + 0.47 \left( \frac{a}{c} \right)^{1.5} \right\} \left( \frac{a}{B} \right)^2, \text{ and} \quad (5)$$

$$\Phi^2 = 1 + 1.464 \left( \frac{a}{c} \right)^{1.65}. \quad (6)$$

Here,  $a$  is the crack length,  $c$  is the crack half width, and  $B$  is the plate thickness. Assuming that the closed-form solution to determine  $K$  for a flat plate in bending in Equation 3 was a reasonable approximation of the curved plate under four-point bending, for a given notch geometry  $K$  is linearly related to the outer fiber stress:

$$K = C_1 \sigma_b. \quad (7)$$

Two starting notch geometries were selected to represent a long-shallow crack and a deep-narrow crack. Table 2 lists the final flaw geometries and their associated initial notch sizes that were prepared by EDM, and the corresponding constant to relate the stress-intensity factor,  $K$  ( $\text{MPa}\sqrt{\text{m}}$ ) to the outer fiber bending stress ( $\text{MPa}$ ).

Table 2 – Flaw type and geometries for CWP test program

Flaw Type	Final Length (mm)	Final Width (mm)	Initial Length (mm)	Initial Width (mm)	$C_1$ ( $\sqrt{\text{m}}$ )
Wide/Shallow	3.0	50	2.4	48.3	0.0843
Narrow/Deep	6.0	30	5.4	24.3	0.0874

Based upon FCGR data from the literature<sup>[6-10]</sup> a stress-intensity factor of between  $15.4 \text{ MPa}\sqrt{\text{m}}$  and  $33.0 \text{ MPa}\sqrt{\text{m}}$  would be required to generate a sufficient fatigue crack growth rate (FCGR). This stress-intensity factor range would provide fatigue crack growth rates between  $0.025 \mu\text{m}$  and  $0.25 \mu\text{m}$  per

cycle<sup>[9-10]</sup>. From the relationship in Equation 7 and the geometry-based constants ( $C_1$ ) in Table 2, the required outer fiber stress would be between 183 MPa and 391 MPa for the aforementioned stress-intensity values at the crack tip.

The data in Table 1 indicated that the loading configuration using the contoured supports for the outer diameter resulted in insufficient stress at the notch location. Use of the straight rollers substantially increased the outer fiber stress into the required range. The final configuration produced an outer fiber stress well in excess of the required values, thus allowing a lower force to be used that resulted in a lower stress elsewhere in the pipe section, which reduced the risk of generating fatigue cracks at the outer edges of the specimen.

An additional advantage to this loading configuration was that the specimen exhibited a local “flattening”, where the curved section of pipe flattened and conformed to the straight profile of the loading rollers, which was believed to have the largest effect on the apparent shift in the neutral plane towards the plate mid-thickness as measured by the strain gages on the I.D. and O.D. surfaces of the pipe. As the neutral plane approached the mid-thickness of the pipe section about the notch, the closed-form solutions for  $K$  presented in Equation 3 became more appropriate.

## MODEL VALIDATION

A finite element analysis (FEA) was performed on the loading configuration of test number 5 (see Table 1) to evaluate the relationship between applied load in bending and stress-intensity factor for a curved plate with a surface flaw. Using commercial software, an implicit, three-dimensional (3-D) finite element model was generated to analyze the CWP specimen in four-point bending. Figure 7 shows a schematic of the FEA model of the CWP specimen. Due to the symmetry, only half of the model was built. The meshes were generated with 27472 linear hexahedral elements of type C3D8RH and 32810 nodes. A  $5.5 \text{ mm} \times 25.0 \text{ mm}$  ( $a \times 2c$ ) notch (an early notch geometry) was modeled at the center of the specimen I.D., and a fine mesh was generated near the flaw region. The contact was defined between the CWP specimen, straight rollers and contoured supports. The bending forces applied in the model were achieved by applying displacement on the straight rollers and fixing the bottom of contoured supports, which was identical to the test condition. Figure 8 shows a plot of the stress-intensity factor versus applied force was calculated from FEA and compared to the results of the linear elastic fracture mechanics (LEFM) based closed-form solution for  $K$  for a flat plate from Equation 3.

The comparison shows that the two models predict the same linear behavior until the force exceeds 350 kN. When the force exceeds 350 kN, the FEA prediction deviates from the LEFM prediction. Divergence was expected because the analytical LEFM solution was elastic, while the FEA was elastic-plastic. As force was increased beyond 350 kN, the FEA prediction

increased at a higher rate than the theoretical linear relation due to plastic deformation at the crack tip. The aforementioned stress-intensity factor between 15.4 MPa√m and 33.0 MPa√m corresponded to a load range of approximately 75 kN to 167 kN. The analytical flat plate solution exhibited excellent agreement with the FEA prediction within this load range. Hence, the FEA results confirm that under the proposed loading arrangement, the closed-form solutions for stress-intensity factor K for flat plates in bending can be used to approximate the K for CWP specimens in bending. It is recognized that the flaw geometry used in the FEA model did not exactly match the flaw size used in the empirical study, but the small differences in flaw size were thought to be irrelevant to the validity of the comparison.

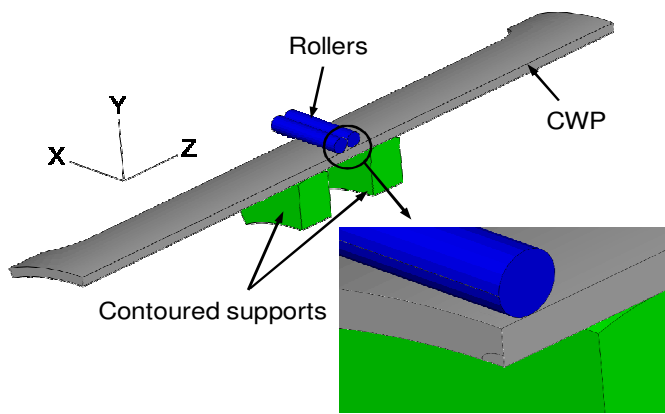


Figure 7 – FEA model of the CWP specimen in four-point bending.

Once a loading configuration and a validated approximation for K had been determined, fatigue pre-cracking of notched base-metal plates commenced. To develop a procedure for accurately fatigue pre-cracking a notched CWP specimen to a specific final flaw size, a few relationships had to be determined. First was the relationship between loading configuration, force and K which has been shown above. Second was to determine the relationship between flaw geometry and a measurable parameter from the loaded plate that would change as the fatigue crack increased in length. Stiffness is a measure of the resistance of a body to elastic deformation and is the inverse of compliance, as the flaw increases in size, the stiffness of the body diminishes and the compliance increases.

### FATIGUE PRE-CRACKING

To elucidate the relationship between flaw size and compliance for the two notch geometries evaluated, several base-metal plates were notched by EDM, according to the flaw sizes listed in Table 2. The plates were fatigue pre-cracked by use of the loading configuration shown in Figure 5, with a 178 mm outer span and 32 mm diameter adjacent straight rollers. The plates

were pre-cracked by use of a stress intensity factor range  $\Delta K = K_{max} - K_{min}$  of 15.4 MPa√m and with a loading ratio  $R = K_{min}/K_{max}$  of 0.4, which was expected to correspond to a fatigue crack growth rate of 0.025 μm per cycle<sup>[9-10]</sup>.

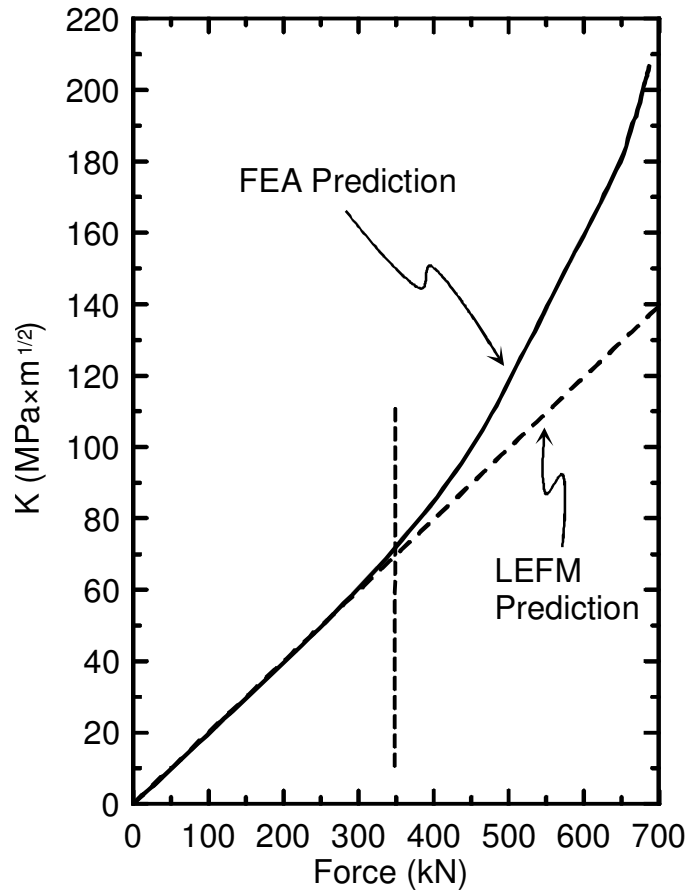


Figure 8 – Predicted stress-intensity factor K at the crack tip versus applied force from the FEA model and the closed-form solution provided from linear elastic fracture mechanics.

Fatigue marker bands were used to correlate the crack length with the number of cycles. The value of  $\Delta K$  during the marker band procedure was maintained at 60 % of the value of  $\Delta K$  used for pre-cracking. The load ratio, R, during the marker band procedure was between 0.4 and 0.44. On some specimens, the lower load ratio resulted in a value of  $K_{max}$  that substantially diminished the fatigue crack growth rate during the marker band step and did not produce visible bands. The lack of visible marker bands is most likely due to a force level that was insufficient to “flatten” the curved plate and thus substantially reduced the applied K.

The pre-cracking procedure consisted of 10,000 cycles at the full  $\Delta K$ , followed by a marker band step at 0.6  $\Delta K$  for 50,000 cycles. The loading frequency was maintained at 12 Hz with a low rate compliance measurement taken every 1000 cycles.

Sufficient loading cycles were applied to extend the crack beyond the target length to provide additional compliance versus crack length data beyond the target length for each of the flaw geometries. After the pre-cracking was complete, the plates were sectioned and the fatigue cracked notch was liberated for fractography and accurate measurement of the crack lengths. Figure 9 shows a scanning electron microscope (SEM) image of a fatigue pre-crack fracture surface from a 5.4 mm long by 28.3 mm wide initial EDM notch. In the fractograph there is evidence of seven distinct marker bands in addition to the initial EDM notch edge (bottom). Also evident is the distinct transition between the fatigue crack and the brittle failure (top), which occurred during the liberation process. From fractographs similar to Figure 9, crack lengths were measured and correlated with compliance data gathered during the pre-cracking procedure.

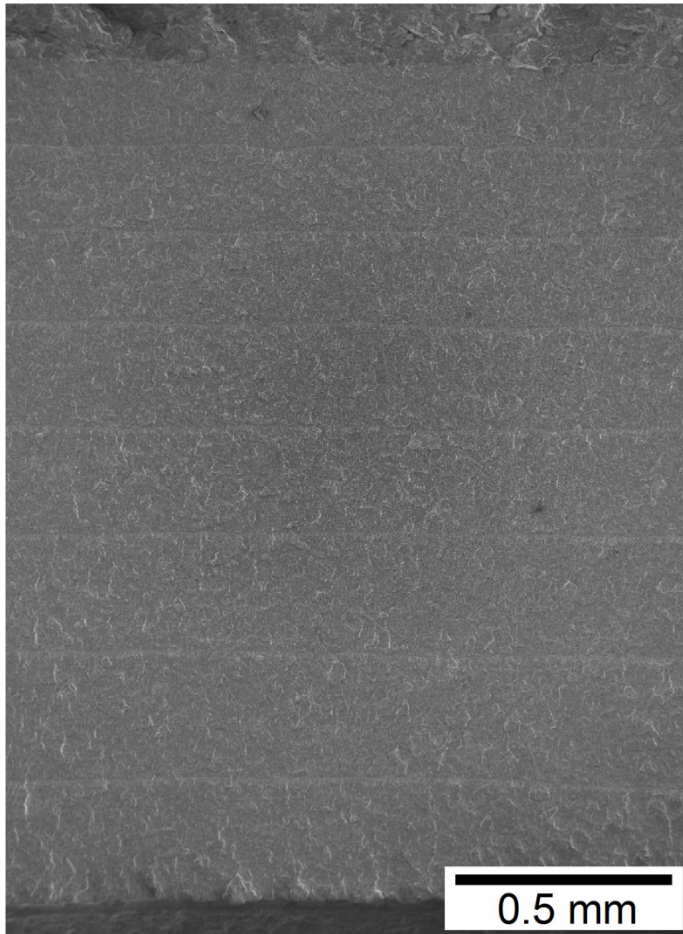


Figure 9 – SEM image of fatigue pre-crack fracture surface showing fatigue marker bands. Initial EDM notch geometry was 5.4 mm deep by 28.3 mm wide.

The plot in Figure 10 shows compliance versus loading cycles for two pre-cracked specimens, one from each notch

configuration. After approximately 10,000 cycles the compliance versus cycles relationship become linear for each notch configuration evaluated. Analysis of the fractographs indicated the non-linear portion of the curve resulted from different crack initiation rates between the deepest point in the EDM notch and at the surface of the EDM notch, which was attributed to the difference in the notch root radii around the EDM notch periphery. The ordinate intercept of the linear portion of the compliance versus cycles data in Figure 10 was termed the compliance intercept,  $C_0$ .

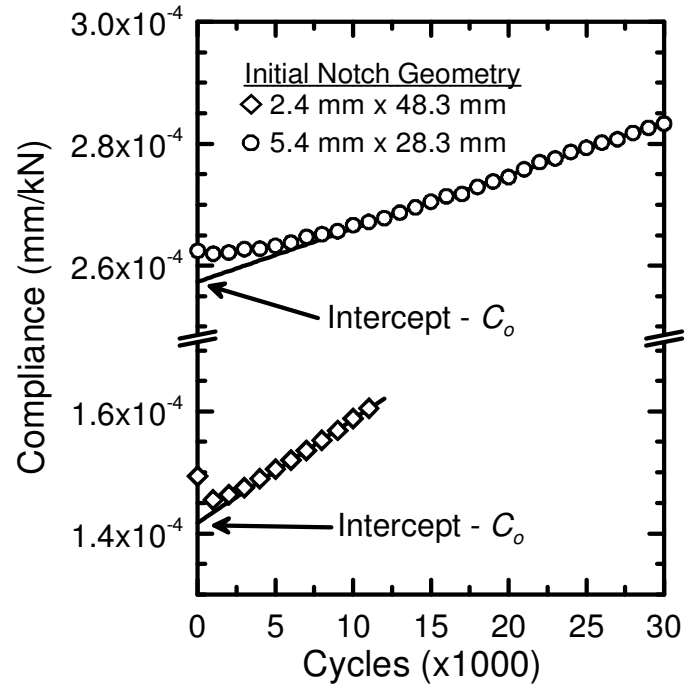


Figure 10 – Compliance versus the number of cycles plot for the two initial notch geometries.

Figure 11 shows the offset compliance versus crack length data measured from fractographs of the pre-cracked fracture surface. The instantaneous compliance  $C_i$ , corresponding to a specific marker band, was offset by the compliance intercept  $C_0$  for each specimen, which removed slight offsets due to minor specimen misalignment with the loading fixtures. The data for the 2.4 mm by 48.3 mm initial notch show excellent linear correlation between lengths of 2.4 mm and 6.0 mm. The data for the 5.4 mm by 28.3 mm initial notch show excellent linearity and repeatability between lengths of 5.2 mm and 6.7 mm, beyond which there exists an increase in slope ( $M_3$ ). The change in slope was believed to be related to a change in flaw shape due to an increased differential in fatigue crack growth rate around the flaw periphery as the deepest part of the crack approached the neutral plane. From the data in Figure 11, the slope of the compliance versus crack length values were determined for the two notch geometries evaluated and the average values are listed in Table 3.

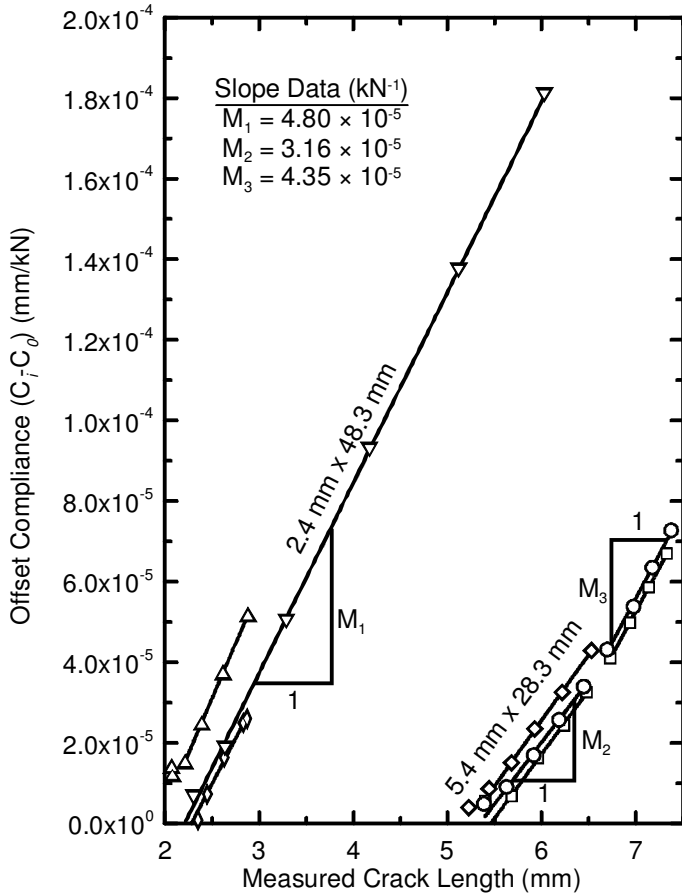


Figure 11 – Compliance *versus* crack length for two surface flaw geometries evaluated.

Table 3 – Slope values of the compliance *versus* crack length

Final Flaw Size (mm)	Initial EDM Notch Size (mm)	Slope M (kN <sup>-1</sup> )
3 x 50	2.4 x 48.3	4.80 x 10 <sup>-5</sup>
6 x 30	5.4 x 28.3	3.16 x 10 <sup>-5</sup>

By use of the characteristic slope values for each geometry listed in Table 3, a predictive formula was developed to accurately predict instantaneous crack lengths during the pre-cracking procedure. For an instantaneous crack length the linear relationship between compliance (C), slope (M), crack length (a), and the intercept (R),

$$C_i = Ma_i + R. \quad (8)$$

When the initial conditions for the pre-cracked plate are known, such as the initial crack length ( $a_0$ ) and an initial compliance ( $C_0$ ), the instantaneous crack length ( $a_i$ ) can be determined from the instantaneous compliance ( $C_i$ ) at that point by

$$a_i = \frac{C_i - C_0}{M} + a_0. \quad (9)$$

A limitation of the predictive formula in Equation 9 is the requisite quality of the initial crack length ( $a_0$ ) and initial compliance ( $C_0$ ) measurements. As shown in Figure 10 the initial response of the compliance to cyclic loading was a transient response which became linear with increased cycles. Numerous attempts to improve the initial compliance measurement improved the repeatability of the transient response. However, the ability to predict the crack length based upon initial measurable compliance values remained less accurate than desired. Fracture surface analysis confirmed that the transient response can be considered to be an artifact of differential crack initiation rates due to different notch root radii around the periphery of the initial EDM notch. The compliance intercept value represents a theoretical initial flaw shape based upon the geometry achieved during steady state fatigue crack growth around the crack periphery. Therefore, the application of the intercept compliance as the initial value in Equation 9 is as a projected value based upon the well behaved linear interrelationships between crack length, compliance, and loading cycles achieved after the transient behavior shown in Figure 10 and steady state fatigue crack growth rate around the notch periphery is achieved.

Figure 12 shows a comparison between predicted crack length values using Equation 9 and measured crack length values to validate the assumptions and evaluate the efficacy of the presented method. The results for the five fatigue pre-crack specimens show that the predicted crack length values are within +/- 2 % of the measured values of crack length. The data in Figure 12 exhibit an excellent linear relationship up to a crack length of about 6.7 mm. At crack lengths in excess of 6.7 mm, the relationship between the predicted crack length and measured crack length for the 5.4 mm by 28.3 mm initial notch had a slope different from that at lengths below 6.7 mm. The deviation from the predictive model is attributed to the change in slope of the compliance versus crack length behavior as shown in the slope change from  $M_2$  to  $M_3$  in Figure 11.

## CONCLUSION

A series of experiments were conducted to evaluate the effects of loading configuration and applied force on the resulting outer fiber stress in a curved plate. Transitioning from uniform bending with contoured loading supports to localized loading with adjacent straight rollers provided sufficient outer fiber stress for fatigue crack growth, reduced the required applied force levels, and reduced the stress levels in the rest of the plate. A comparison of the stress intensity factor, K, predictions for a surface flaw based upon linear elastic fracture mechanics for a flat plate and finite element analysis model of the CWP specimen in bending showed excellent agreement within the force range used in the present study and validated the applicability of the closed-form solution for determining K.

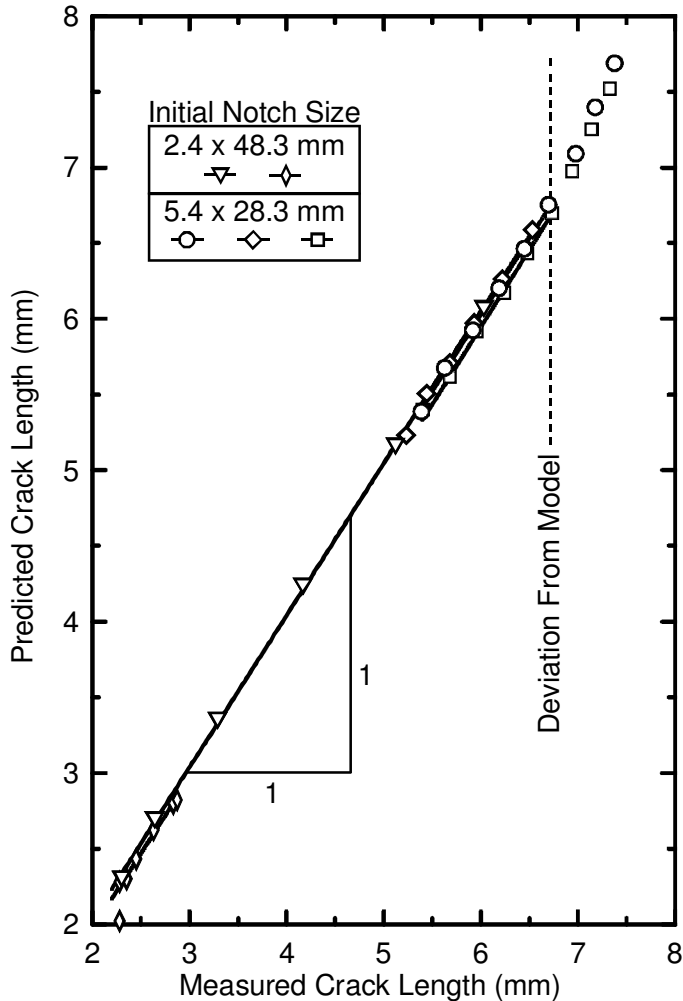


Figure 12 – Predicted versus actual crack lengths for both initial notch configurations using the compliance intercept method.

A method was developed to enable the accurate and repeatable extension of a machined surface notch by fatigue pre-cracking in bending to a pre-determined length for subsequent fracture mechanics testing on a curved wide plate specimen in tension. The method was based upon the empirically determined relationship between compliance and crack length for the two flaw geometries. It was shown that crack length could be accurately predicted from instantaneous measurements of compliance when the relationship between compliance and crack length for a given flaw geometry, the initial flaw size, and projected compliance intercept were all known.

#### ONGOING/FUTURE WORK

At the time of this writing, the researchers have been exploring the limits of notch geometry on the applicability of this method; for the same pipe diameter, thickness and steel grade. Another analysis has begun to further optimize the loading configuration and extend the limits of notch geometries. Other pipe

geometries and subsequent notch geometries are being considered for future work. Additionally, comparisons between fatigue pre-cracking in bending and in tension are being considered for this and other pipe geometries.

#### ACKNOWLEDGMENTS

The authors acknowledge the help and support of colleagues at NIST in Boulder, CO, and in particular, Dr. Nicholas Barbosa for his help with imaging the fracture surfaces, Dr. David Read for his discussions on the introduction of marker bands, and Messrs. Ross Rentz and Marc Dvorak for their assistance.

#### REFERENCES

- [1] N.-S. Huh, Y.-J. Kim, J.-B. Choi, Y.-J. Kim, and C.-R. Pyo, 2004, "Prediction of Failure Behavior for Nuclear Piping Using Curved Wide-Plate Test," *Journal of Pressure Vessel Technology*, 126, pp. 419-425.
- [2] Y.-Y. Wang, M. Liu, Y. Chen, and D. Horsley, 2006, "Effects of Geometry, Temperature, and Test Procedure on Reported Failure Strains from Simulated Wide Plate Tests," *Proc. 6<sup>th</sup> International Pipeline Conference*, paper No. 10497, Calgary, Alberta, Canada.
- [3] D.P. Fairchild, W. Cheng, S.J. Ford, K. Minnaar, N.E. Biery, A. Kumar, and N.E. Nissley, 2007, "Recent Advances in Curved Wide Plate Testing and Implications for Strain-Based Design," *Proc. 7<sup>th</sup> International Offshore and Polar Engineering Conference*, Lisbon, Portugal, pp. 3013-3022.
- [4] Y.-Y. Wang, M. Liu, and D. Rudland, 2007, "Strain Based Design of High Strength Pipelines," *Proc. 7<sup>th</sup> International Offshore and Polar Engineering Conference*, Lisbon, Portugal, pp. 3186-3193.
- [5] J.C. Newman and I.S. Raju, 1979, "Analyses of Surface Cracks in Finite Plates Under Tension or Bending Loads," *NASA Technical Paper No. 1578*.
- [6] J.M. Treinen, Ph.P. Darcis, J.D. McColskey, R. Smith and J. Merritt, 2008, "Effects of Specimen Geometry on Fatigue-Crack Growth Rates in Pipeline Steels," *Proc. 7<sup>th</sup> International Pipeline Conference*, paper No. 64360, Calgary, Alberta, Canada.
- [7] Ph. P. Darcis, J.M. Treinen, and J.D. McColskey, Nov. 2009, "Fatigue Crack Growth Rates in Pipeline Steels Using Curved M(T) Specimens," *Journal of Testing and Evaluation*, 37 [6], pp. 511-519.
- [8] A. Bussiba, Ph. P. Darcis, J.D. McColskey, C.N. McCowan, T.A. Siewert, G. Kohn, R. Smith, and J. Merritt, 2006, "Fatigue Crack Growth Rates in Six Pipeline Steels," *Proc. 6<sup>th</sup> International Pipeline Conference*, paper No. 10320, Calgary, Alberta, Canada.
- [9] J.M. Barsom, Nov. 1971, "Fatigue-Crack Propagation in Steels of Various Yield Strengths," *Transactions of the ASME, Journal of Engineering for Industry, Series B*, 93 [4], pp. 1190-1196.
- [10] J.M. Barsom and S.T. Rolfe, 1987, *Fracture & Fatigue Control in Structures*, 2<sup>nd</sup> Ed., Prentice-Hall, Inc., Englewood Cliffs, New Jersey, pp. 290-291.